Green Synthesis of Yellow-fluorescent Carbon Nano-Dots for Cancer-Cell Image and Photocatalytic Inactivation by Using Microplasma

Jie He (hejie2310@126.com)
Shanghai 9th Peoples Hospital Affiliated to Shanghai Jiaotong University School of Medicine
Xing Qin
Shanghai 9th Peoples Hospital Affiliated to Shanghai Jiaotong University School of Medicine
Jinlin Liu
Shanghai 9th Peoples Hospital Affiliated to Shanghai Jiaotong University School of Medicine
Qing Zhang
Shanghai Jiaotong University: Shanghai Jiao Tong University
Wantao Chen
Shanghai 9th Peoples Hospital Affiliated to Shanghai Jiaotong University School of Medicine
Xiaoxia Zhong
Shanghai Jiaotong University: Shanghai Jiao Tong University

Nano Express

Keywords: atmospheric pressure micro plasma, bioimage, carbon quantum dots, photodynamic therapy, yellow emission

Posted Date: October 2nd, 2020

DOI: https://doi.org/10.21203/rs.3.rs-84467/v1

Version of Record: A version of this preprint was published on January 21st, 2021. See the published version at https://doi.org/10.1186/s11671-021-03478-2.

Green Synthesis of Yellow-fluorescent Carbon Nano-dots for cancer-cell image and photocatalytic inactivation by using microplasma

Xing Qin [1, 2, #], Jinlin Liu [3, #], Qing Zhang [4], Wantao Chen [1, 2], Jie He [1, 2, *], Xiaoxia Zhong [4, *]

Affiliation of the authors:

[1] Department of Oral and Maxillofacial-Head and Neck Surgery, Ninth People's Hospital, Shanghai Jiao Tong University School of Medicine, Shanghai, 200011, PR China.

[2] Shanghai Key Laboratory of Stomatology & Shanghai Research Institute of Stomatology; National Clinical Research Center of Stomatology. Shanghai, 200011, PR China.

[3] Hunan Key Laboratory of Oral Health Research & Hunan 3D Printing Engineering Research Center of Oral Care & Hunan Clinical Research Center of Oral Major Diseases and Oral Health & Xiangya Stomatological Hospital & Xiangya School of Stomatology, Central South University,Changsha, Hunan, 410008, PR China.

[4] State Key Laboratory of Advanced Optical Communication Systems and Networks, Key Laboratory for Laser Plasmas (Ministry of Education), Department of Physics and Astronomy, Shanghai Jiao Tong University, Shanghai 200240, PR China.

[#] **These authors contributed equally to this work.**

*** Corresponding Authors:**

Xiaoxia Zhong, State Key Laboratory of Advanced Optical Communication Systems and Networks, Key Laboratory for Laser Plasmas (Ministry of Education), Department of Physics and Astronomy, Shanghai Jiao Tong University, Shanghai 200240, China; Email: xxzhong@sjtu.edu.cn.

Jie He, Ninth People's Hospital, Shanghai Jiao Tong University School of Medicine, 639 Zhizaoju Road, Shanghai 200011, China; E-mail: hejie2310@126.com.

E-mail address:

Xing Qin: xingzaing@foxmail.com

Jinlin Liu: liujinlin2017@csu.edu.cn

Qing Zhang: qingzhang@sjtu.edu.cn

Wantao Chen: chenwantao196323@sjtu.edu.cn

Jie He: hejie2310@126.com

Xiaoxia Zhong: xxzhong@sjtu.edu.cn

Abstract:

In recent years, multifunctional nanoparticles with combined diagnostic and therapeutic functions show great promise in nanomedicine. In this work, we report the environmentally friendly synthesis of fluorescent carbon nano-dots such as carbon quantum dots (CQDs) by microplasma using o-phenylenediamine. The produced CQDs exhibited a wide absorption peaks at 380-500 nm and emitted bright yellow fluorescence with a peak at 550 nm. The CQDs were rapidly taken up by HeLa cancer cells. When excited under blue light, a bright yellow fluorescence signal and intense reactive oxygen species (ROS) were efficiently produced, enabling simultaneous fluorescent cancer cell imaging and photodynamic inactivation, with a 40% decrease in relative cell viability. Furthermore, the CQDs has 98% cell viability at concentrations of 400 $\mu g \cdot mL^{-1}$ in the dark demonstrating excellent biocompatibility. The newly prepared CQDs are thus demonstrated to be materials that can be effectively for imaging-guided cancer therapy.

Keywords: atmospheric pressure micro plasma; bioimage; carbon quantum dots; photodynamic therapy; yellow emission

Introduction

Cancer remains a leading cause of death worldwide[1]. Multifunctional nanoparticles with both diagnostic and therapeutic functions have promising applications in nanomedicine. Simultaneous image-guided therapy is a new concept in cancer treatment and shows promise with respect to the optimization of therapeutic efficiency. It can provide useful information regarding the size and location of tumors, the optimal time window for phototherapy, and therapeutic efficacy[2-4]. Photodynamic therapy (PDT) is used to treat many kinds of cancer and other diseases owing to its spatiotemporal selectivity and non-invasive nature[5, 6]. Ideal photosensitizers generally possess the following characteristics: (1) highly efficient generation of reactive oxygen species (ROS), (2) good biocompatibility, and (3) water solubility[7]. However, current applications of PDT are limited by the poor water solubility, instability, and sub-optimal excitation wavelengths of photosensitizers. Therefore, the generation of photosensitizer substitutes with good water-solubility and biocompatibility by environmentally friendly and low-cost methods is needed.

Carbon quantum dots (CQDs) have received tremendous attention owing to their unique beneficial properties, such as simple and environmentally friendly synthesis, low toxicity, excellent water solubility and light stability[8]. CQDs have potential uses in cellular imaging, biosensing, targeted drug delivery, and other biomedical applications[9-13]. There are two major approaches for the synthesis of carbon dots, bottom-up and top-down approaches. Top-down methods include electrochemical oxidation, laser ablation, chemical oxidation, and ultrasonic synthesis methods.

Bottom-up methods consist of hydrothermal treatment, microwave synthesis, and thermal decomposition[14-17]. However, the high temperature, high pressure, and strong acids required lead to substantial energy consumption, complicated processes, and unavoidable harm to the environment. Moreover, CQDs can be produced within just a few minutes using a microplasma-liquid method without high temperature condition, large energy input, and laborious procedures[18-20]. Microplasmas supply a unique physicochemical environment to both fundamental studies and applications involving advanced materials. The chemical and electronic environments provided by the microplasmas are highly nonequilibrium and can store energy. In this environment, a large number of electrons, ions, free radicals, and other excited, ionized, and other types of active substances can be produced[21, 22]. Although o-phenylenediamine is used as raw material to synthesize carbon nano dots, it has not been used in microplasma synthesis[23-25].

In this study, o-phenylenediamine was used as a raw material to synthesize CQDs by micro plasma treatment. The CQDs generated by this method were uniform in size (around 3.2 nm in diameter) and exhibited an emission peak at around 550 nm. We demonstrated that the newly synthesized CQDs could produce a large amount of ROS under light conditions. In vitro, CQDs could be absorbed by HeLa tumor cells and emitted yellow light under blue wavelength excitation at 420-500 nm with low toxicity. We also observed the inactivation of HeLa tumor cells under irradiation at 460 nm. These results suggest that the newly prepared CQDs are promising materials for imaging-guided or targeted cancer therapy.

Results and Discussion

Characterization of CQDs

The yellow-emissive CQDs could be prepared in a facile and environmentally friendly manner by a micro plasma method using o-phenylenediamine as the carbon precursor. **Figure 1A** shows transmission electron microscope (TEM) images of the CQD particles. The particles produced by micro plasma were cyclo-sharp or oval-shaped with an average diameter of 3.2 nm. As shown in the high-resolution image **Figure 1A** (inset), the lattice distance in the CQDs is 0.21 nm, belonging to the (1,1,0) plane of graphite. The Raman spectrum shown in **Figure 1E**, as a result of sp3 and sp2-hybridization of carbon, D mode, named as disorder induced mode, located around 1342 cm-1 and G mode centers around 1507 cm^{-1} respectively. It is known that the intensity of D mode compared with G mode depends on the size of the graphite micro-crystals in the sample. The higher disorder of the sample leads to the higher intensity ratio of ID/IG and the smaller the graphite micro-crystal. The D and G mode of CQD powders can be viewed as small graphite flakes with a relatively high intensity ratio ID/IG (0.77).

FTIR and XPS are powerful tools to characterize the chemical composition and structure of carbon-based materials. FTIR data for CQDs were recorded in the range of 400-4000 cm^{-1}, as shown in **Figure 1F**. The FTIR spectrum revealed that the CQDs mainly contain amine (3052 and 3324 cm^{-1}), OH (3200 cm^{-1}), C=O (1595 cm^{-1}), C-N/C-O (1200 cm^{-1}), C=C (1500 cm^{-1}), and CH (748 cm^{-1}) functional groups or chemical bonds[26, 27]. The surface components of the CQDs, as determined by XPS, were consistent with the FTIR results. The full spectrum presented in **Figure 2A** showed

three typical peaks: C 1s (285 eV), N 1s (400 eV), and O 1s (531 eV).

As shown in Figure 2B-D, a C 1s analysis revealed the presence of sp2/sp3 carbons (C-C/C=C, 284.8 eV), nitrous carbons (C-O/C-N, 285.9 eV), and carbonyl carbons (C=O, 287.7 eV). The N 1s band was deconvoluted into three peaks at 399.3, 400.3, and 401.7 eV, which correspond to pyrrolic N, graphitic N, and amino N, respectively. The O 1s band contained peaks at 531.6 and 533.1 eV for C-O and C=O, respectively[28, 29]. Furthermore, the optical properties of CQDs were investigated using fluorescence spectroscopy and UV-Vis absorption. The fluorescence emission spectra of CQDs are shown in **Figure 1C**. The prepared CQDs exhibit an excitation-dependent fluorescence emission behavior. When excited at wavelengths from 400 to 500 nm, the maximum fluorescence emission peak red-shifted from 473 to 519 nm and the fluorescence intensity decreased sharply[30]. As shown in **Figure 1D**, the UV-vis spectra of CQD features a strong absorption peak in the wavelength range of 400-490 nm. The CQDs exhibited two characteristic absorption peaks at 280 and 420 nm, which can be assigned to π–π* (aromatic C=C) and n–π* (carboxyl and/or C-N) transitions, respectively[31, 32]. Therefore, These optical properties of CQDs provide feasibility for simultaneous biological imaging and photodynamic inactivation.

Bioimaging and cytotoxicity of CQDs

To assess the capability of CQDs for bioimaging and cell labeling, *in vitro* cellular imaging using CQDs was investigated on HeLa cells by CLSM and illustrated in **Figure 3A**, HeLa cells showed bright yellow fluorescence evenly distributed throughout the

cell. It should be noted that low CQDs concentration of 200 μg·mL^{-1} was required for these cell imaging experiments for the bio-fluorescence labeling of HeLa cancer cells. The as-prepared CQDs are accordingly a potential bio-labelling reagent. For biomedical applications, materials must be highly biocompatible at recommended dosages. To examine cytotoxicity, HeLa cells were treated with CQDs at final concentrations ranging from 0 to 400 μg·mL^{-1} for 24 h. As shown in **Figure 3B**, over 95% of cells survived, as determined by MTT assays. These data suggest that the newly generated CQDs have low cytotoxicity and high biocompatibility.

Efficacy of photodynamic therapy

Cancer cell inactivation

As shown in **Figure 3C**, viability did not differ between HeLa cells treated with CQDs or blue light alone. Simultaneous treatment with CQDs and blue light markedly reduced cell viability, depending on the duration of photo-exposure. After irradiation at 460 nm for 15 min, the CQDs displayed remarkable antitumor activity; the viability of HeLa cells decreased by about 40% at a concentration of 200 μg·mL^{-1}. These results indicate that the CQDs were as effective as some clinical anticancer drugs, like Photofrin[33].

ROS generation of CQDs

During PDT, cancer cells can be killed by cytotoxic ROS generated by the endocytosed photosensitizer under appropriate irradiation conditions[34, 35]. ROS can inactivate target cells by apoptosis or necrosis with little side effects via PDT in several diseases[36-39]. Inspection of **Figure 4A** shows that ROS reagent emits red

fluorescence, indicating the generation of ROS, which is well overlapped with the fluorescence of CQDs. As shown in **Figure 4B**, compared with the control and no laser irradiation groups, the experimental groups under 460 nm laser irradiation for 15 min showed obvious ROS generation. Our results indicating that CQDs could significantly promote the production of the intracellular ROS under the irradiated of 460 nm laser and have great potential for application in PDT. As shown in **Figure 4C**, the CQDs can be excited from the ground state (S0 in **Figure 4C**) to an excited state (Sn in **Figure 4C**), and the efficiency of this process is determined by the intensity of the light source and the extinction coefficient. After solvent-mediated relaxation, CQDs remain at the lowest vibration level of the first singlet excited state. Due to the rapid vibrational relaxation following excitation, the energy of the photon emitted from the first singlet excited state (S1 in **Figure 4C**) is lower than the energy of the excitation photon, resulting in a wavelength increase. Fluorescence imaging utilizes the CQDs transition from S0 to Sn to S1[40]. The CQDs were ingested by HeLa tumor cells and emit fluorescence when illuminated by a suitable wavelength source, thereby allowing the cells to be labeled. S1 can return to the S0 state by fluorescence or by intersystem crossing to a non-fluorescent triplet excited state (T1 in Figure 4C) [41, 42]. The fluorescent group of T1 is especially active in electron transfer reactions, generating superoxide free radicals and subsequently resulting in fluorescent group degradation. The energy from T1 transferred to molecular oxygen would produce an excited singlet oxygen oxidizing agent that is stronger than ground state molecular oxygen. The superoxide radicals and singlet oxygen, as well as other ROS, including OH and H_2O_2,

react with nearby biological molecules to exert phototoxicity, leading to cell death. After the CQDs are taken up by HeLa cells, illumination results in the transfer of the singlet state to the triplet state through the intersystem, and the process of energy transfer produces ROS and ultimately results in cell death. Under the appropriate wavelength source, the CQDs undergo two types of energy transfer. Fluorescence is emitted to mark HeLa tumor cells, and HeLa cells are killed by ROS. Our experimental data indicate the good biocompatibility of the newly produced CQDs in the dark and the inactivation efficiency of tumor cells under light conditions. Hence, the CQDs could be used as a photosensitizer for tumor cells and tissues.

Conclusions

In summary, we synthesized photoluminescent CQDs using o-phenylenediamine by the plasma method. Excited by a blue laser, CQDs with a diameter of about 3.2 nm emit yellow fluorescence. Raman, UV-vis, FTIR, and XPS results showed that more carbon atoms were involved in sp2 hybridization, forming a new organic group. CQDs synthesized by the plasma method proved to be an effective biomarker in cell imaging experiments. The fluorescence emitted by CQDs can clearly mark HeLa cells. Our results show the photodynamic cytotoxicity of carbon quantum dots in vitro, supporting their application in PDT.

Experimental Methods

Synthesis of carbon quantum dots

The micro plasma processing system is summarized in **Figure S1**. A hollow stainless pipe with an inner diameter of 180 μm was connected to a high-voltage direct current power source (Tianjin Dongwen High-Voltage Supply Co., Ltd., Tianjin, China) and was kept at 2 mm above the surface of the solution. A Pt electrode (DJS-1; Shanghai INESA Scientific Instrument Co., Ltd., Shanghai, China) was connected to the cathode of the power source and immersed in the solution. Then, 400 mg of o-phenylenediamine (Shanghai, China) was dissolved in 40 mL of deionized water, and 20 mL of the o-phenylenediamine solution was added to a Petri dish and stirred using a magnetic stirrer. During micro plasma treatment, argon (Ar) gas flowed through the pipe at a flow rate of 60 sccm, and the DC current was kept at 17 mA. After 10 min of plasma treatment, the brownish-black product was dialyzed using a dialysis membrane (molecular weight cut-off, 500 Da) against 2 L of deionized water for 12 h and subsequently filtered through a 0.22 μm ultrafiltration membrane. Finally, pure CQDs were obtained by freeze drying.

Characterization of the structure, composition, and optical properties of CQDs

The size and morphology of the CQDs were characterized by TEM using a JEM-2100F system (JEOL, Tokyo, Japan). Fluorescence spectroscopy was performed using a Perkin Elmer LS 55 Luminescence Spectrometer (Waltham, MA, USA). The UV/Vis absorption spectra were measured using the Varian Cary 50 UV-VIS spectrophotometer (Palo Alto, CA, USA). FTIR spectra were obtained using a Nicolet 6700 spectroscope (Thermo Scientific, Waltham, MA, USA), and Raman spectroscopy was performed

using the 800 UV micro-Raman spectrometer (Invia-reflex, UK). XPS experiments were performed using an Axis Ultra DLD system (Shimadzu/Kratos Analytical Ltd., Kyoto, Japan).

Cell culture and cytotoxicity assay

HeLa cells (ATCC, Manassas, VA, USA) were cultured at 37°C in Dulbecco's Modified Eagle Medium (DMEM) containing 10% FBS and 1% penicillin–streptomycin. For cytotoxicity studies, cells were counted and seeded in 96-well plates containing 200 μL of complete medium at a density of 6000 cells per well. After 24 h of culture, cells were treated with CQDs at concentrations of 0, 25, 50, 100, 200, and 400 $\mu g \cdot mL^{-1}$ for another 24 h to assess cytotoxicity. These solutions were then replaced with 100 μL of MTT (3-(4,5-dimethylthiazolyl-2-yl)-2,5-diphenyltetrazolium bromide) test solution and incubated for 4 h in an incubator in the dark. The supernatant was removed and the crystals were dissolved in dimethyl sulfoxide (DMSO). Absorbance was measured at 490 nm. The optical density was related to cell viability by assuming 100% viability for the control sample without CQDs.

Cell imaging

Cells at a concentration of $2 \times 104\ mL^{-1}$ were seeded in a confocal dish (diameter = 15 mm), cultured for 24 h, and washed with PBS twice to ensure no dead cells. A CQD solution (200 $\mu g \cdot mL^{-1}$; pH = 7) was added and the cells were incubated for 6 h. The cells were subsequently washed with PBS three times to remove unbound CQDs and

fixed with 4% paraformaldehyde. Then, the samples were observed using a confocal laser scanning microscope (CLSM, LSM510, Zeiss, Germany) with excitement at wavelengths ranging from 400 to 450 nm.

Photodynamic therapy and ROS measurement

To investigate antitumor effects, HeLa cells were incubated with CQDs at 200 μg·mL^{-1} for 24 h at 37°C in the dark and treated with light at 460 nm (30 mW·cm−2) for 5, 10 and 15 min. After 24 h of incubation, a standard MTT assay was performed to determine the relative cell viability. The intracellular generation of ROS was detected chemically using the spectrophotometric method with Fluorometric Intracellular Ros Assay Kit (sigma, USA). Cells were cultured in a confocal dish (diameter = 15 mm) overnight for cell attachment. Then, the cells were incubated with CQDs for 4 h at 200 μg·mL^{-1}. Subsequently, added 100 μL/well of Master Reaction Mix. After incubation for 1h, the cells were fixed with 4% paraformaldehyde for 10 min, Fluorescence images of the cells were observed by CLSM. Regarding ROS production detection, Cells were cultured in 96-well plates with 200 μL culture medium, after 24 h incubation, the medium was replaced with 100 μL CQDs solution at 0, 100, 200 μg·mL^{-1}. The cells were then incubated for further 4 h. Subsequently, they were washed three times with PBS and with or without irradiation for 15 min, added 100 μL/well of Master Reaction Mix. After incubation for 1h, the fluorescence intensity was detected using a fluorescence reader (520 nm excitation, 605 nm emission).

List of abbreviations

PDT, Photodynamic therapy; ROS, Reactive oxygen species; CQDs, Carbon quantum dots; TEM, Transmission electron microscope; DMEM, Dulbecco's modified eagle medium; MTT, 3-(4,5-dimethylthiazolyl-2-yl)-2,5-diphenyltetrazolium bromide; DMSO, dimethyl sulfoxide.

Availability of data and materials

All data and materials of the current study are available from the corresponding author on reasonable request.

Competing interests

The authors declare that they have no competing interests.

Funding

This work was financially supported by the National Natural Science Foundation of China (Grant No. 31400859 and 11675109), Shanghai Natural Science Foundation (19ZR1429900) and Shanghai Municipal Commission of Health and Family Planning Foundation (201840021).

Authors' contributions

XXZ, JH and WTC contributed to the conception and design. XXZ and QZ contributed to the synthesis of carbon nano-dots. XQ, JLL and QZ contributed to the characteristic

analysis of the CQDs. XQ and JLL participated in the cell experimentation, analysis and interpretation of data. XQ, JLL, WTC, JH and XXZ contributed to the writing and/or revision of the manuscript. All authors have read and approved the final manuscript.

Acknowledgements

Not applicable.

References

1. Bray F, Ferlay J, Soerjomataram I, Siegel RL, Torre LA, and Jemal A. Global cancer statistics 2018: GLOBOCAN estimates of incidence and mortality worldwide for 36 cancers in 185 countries. CA Cancer J Clin. 2018; 68(6): 394-424.
2. Shen J, Zhao L, and Han G. Lanthanide-doped upconverting luminescent nanoparticle platforms for optical imaging-guided drug delivery and therapy. Adv Drug Deliv Rev. 2013; 65(5): 744-55.
3. de Jong M, Essers J, and van Weerden WM. Imaging preclinical tumour models: improving translational power. Nat Rev Cancer. 2014; 14(7): 481-93.
4. Lammers T, Aime S, Hennink WE, Storm G, and Kiessling F. Theranostic nanomedicine. Acc Chem Res. 2011; 44(10): 1029-38.
5. Oniszczuk A, Wojtunik-Kulesza KA, Oniszczuk T, and Kasprzak K. The potential of photodynamic therapy (PDT)-Experimental investigations and clinical use. Biomed Pharmacother. 2016; 83: 912-29.
6. Monro S, Colon KL, Yin H, Roque J, 3rd, Konda P, Gujar S*, et al.* Transition Metal Complexes and Photodynamic Therapy from a Tumor-Centered Approach: Challenges, Opportunities, and Highlights from the Development of TLD1433. Chem Rev. 2019; 119(2): 797-828.
7. Lovell JF, Liu TW, Chen J, and Zheng G. Activatable photosensitizers for imaging and therapy. Chem Rev. 2010; 110(5): 2839-57.
8. Ghosal K and Ghosh A. Carbon dots: The next generation platform for biomedical applications. Mater Sci Eng C Mater Biol Appl. 2019; 96: 887-903.
9. Mishra V, Patil A, Thakur S, and Kesharwani P. Carbon dots: emerging theranostic nanoarchitectures. Drug Discov Today. 2018; 23(6): 1219-32.
10. Liu W, Li C, Ren Y, Sun X, Pan W, Li Y*, et al.* Carbon dots: surface engineering and applications. J Mater Chem B. 2016; 4(35): 5772-88.

11. Zhang L, Wang D, Huang H, Liu L, Zhou Y, Xia X*, et al.* Preparation of Gold-Carbon Dots and Ratiometric Fluorescence Cellular Imaging. ACS Appl Mater Interfaces. 2016; 8(10): 6646-55.
12. Yuan Y, Guo B, Hao L, Liu N, Lin Y, Guo W*, et al.* Doxorubicin-loaded environmentally friendly carbon dots as a novel drug delivery system for nucleus targeted cancer therapy. Colloids Surf B Biointerfaces. 2017; 159: 349-59.
13. Du J, Xu N, Fan J, Sun W, and Peng X. Carbon Dots for In Vivo Bioimaging and Theranostics. Small. 2019; 15(32): e1805087.
14. Sun YP, Zhou B, Lin Y, Wang W, Fernando KA, Pathak P*, et al.* Quantum-sized carbon dots for bright and colorful photoluminescence. J Am Chem Soc. 2006; 128(24): 7756-7.
15. Dong X, Shi Y, Huang W, Chen P, and Li LJ. Electrical detection of DNA hybridization with single-base specificity using transistors based on CVD-grown graphene sheets. Adv Mater. 2010; 22(14): 1649-53.
16. Xu X, Ray R, Gu Y, Ploehn HJ, Gearheart L, Raker K*, et al.* Electrophoretic analysis and purification of fluorescent single-walled carbon nanotube fragments. J Am Chem Soc. 2004; 126(40): 12736-7.
17. Du F, Ming Y, Zeng F, Yu C, and Wu S. A low cytotoxic and ratiometric fluorescent nanosensor based on carbon-dots for intracellular pH sensing and mapping. Nanotechnology. 2013; 24(36): 365101.
18. Wang Q ZQ, Chen Y, et al. . Blue luminescent amorphous carbon nanoparticles synthesized by microplasma processing of folic acid. Plasma Process Polym. 2018; 15.
19. Huang X, Li Y, Zhong X, Rider AE, and Ostrikov KK. Fast Microplasma Synthesis of Blue Luminescent Carbon Quantum Dots at Ambient Conditions. Plasma Processes and Polymers. 2015; 12(1): 59-65.
20. Lin L and Wang Q. Microplasma: A New Generation of Technology for Functional Nanomaterial Synthesis. Plasma Chemistry and Plasma Processing. 2015; 35(6): 925-62.
21. Chiang WH, Mariotti D, Sankaran RM, Eden JG, and Ostrikov K. Microplasmas for Advanced Materials and Devices. Advanced Materials. 2019.
22. Mariotti D, Patel J, Švrček V, and Maguire P. Plasma-Liquid Interactions at Atmospheric Pressure for Nanomaterials Synthesis and Surface Engineering. Plasma Processes and Polymers. 2012; 9(11-12): 1074-85.
23. Zhang S, Ji X, Liu J, Wang Q, and Jin L. One-step synthesis of yellow-emissive carbon dots with a large Stokes shift and their application in fluorimetric imaging of intracellular pH. Spectrochimica Acta Part A: Molecular and Biomolecular Spectroscopy. 2020; 227.
24. Tian M, Liu Y, Wang Y, and Zhang Y. Facile synthesis of yellow fluorescent carbon dots for highly sensitive sensing of cobalt ions and biological imaging. Analytical Methods. 2019; 11(32): 4077-83.
25. Tian M, Liu Y, Wang Y, and Zhang Y. Yellow-emitting carbon dots for selective detecting 4-NP in aqueous media and living biological imaging. Spectrochim

Acta A Mol Biomol Spectrosc. 2019; 220: 117117.
26. Fang HY, Huang WM, and Chen DH. One-step synthesis of positively charged bifunctional carbon dot/silver composite nanoparticles for killing and fluorescence imaging of Gram-negative bacteria. Nanotechnology. 2019; 30(36): 365603.
27. Zhang Y, Ishikawa K, Mozetič M, Tsutsumi T, Kondo H, Sekine M, *et al.* Polyethylene terephthalate (PET) surface modification by VUV and neutral active species in remote oxygen or hydrogen plasmas. Plasma Processes and Polymers. 2019; 16(6).
28. Lu S, Sui L, Liu J, Zhu S, Chen A, Jin M, *et al.* Near-Infrared Photoluminescent Polymer-Carbon Nanodots with Two-Photon Fluorescence. Adv Mater. 2017; 29(15): 1603443.
29. Jiang K, Sun S, Zhang L, Wang Y, Cai C, and Lin H. Bright-Yellow-Emissive N-Doped Carbon Dots: Preparation, Cellular Imaging, and Bifunctional Sensing. ACS Applied Materials & Interfaces. 2015; 7(41): 23231-8.
30. Libin Tang, Rongbin Ji, Xiangke Cao, and Jingyu Lin HJ, Xueming Li, Kar Seng Teng, Chi Man Luk, Songjun Zeng, Jianhua Hao, and Shu Ping Lau Deep Ultraviolet Photoluminescence of Water-Soluble Self-Passivated Graphene Quantum Dots. ACS nano. 2012; 6: 5102-10.
31. Wang L and Zhou HS. Green synthesis of luminescent nitrogen-doped carbon dots from milk and its imaging application. Anal Chem. 2014; 86(18): 8902-5.
32. Xu M, He G, Li Z, He F, Gao F, Su Y, *et al.* A green heterogeneous synthesis of N-doped carbon dots and their photoluminescence applications in solid and aqueous states. Nanoscale. 2014; 6(17): 10307-15.
33. Beack S, Kong WH, Jung HS, Do IH, Han S, Kim H, *et al.* Photodynamic therapy of melanoma skin cancer using carbon dot – chlorin e6 – hyaluronate conjugate. Acta Biomaterialia. 2015; 26: 295-305.
34. Jin Y, Li Y, Ma X, Zha Z, Shi L, Tian J, *et al.* Encapsulating tantalum oxide into polypyrrole nanoparticles for X-ray CT/photoacoustic bimodal imaging-guided photothermal ablation of cancer. Biomaterials. 2014; 35(22): 5795-804.
35. Li Y, Liu Z, Hou Y, Yang G, Fei X, Zhao H, *et al.* Multifunctional Nanoplatform Based on Black Phosphorus Quantum Dots for Bioimaging and Photodynamic/Photothermal Synergistic Cancer Therapy. ACS Appl Mater Interfaces. 2017; 9(30): 25098-106.
36. Rkein AM and Ozog DM. Photodynamic therapy. Dermatol Clin. 2014; 32(3): 415-25, x.
37. Aniogo EC, Plackal Adimuriyil George B, and Abrahamse H. The role of photodynamic therapy on multidrug resistant breast cancer. Cancer Cell International. 2019; 19(1).
38. Hwang HS, Shin H, Han J, and Na K. Combination of photodynamic therapy (PDT) and anti-tumor immunity in cancer therapy. J Pharm Investig. 2018; 48(2): 143-51.
39. Shi X, Zhang CY, Gao J, and Wang Z. Recent advances in photodynamic therapy for cancer and infectious diseases. Wiley Interdiscip Rev Nanomed

Nanobiotechnol. 2019; 11: e1560.
40. Turro NJ, Ramamurthy V, and Scaiano JC. Modern Molecular Photochemistry of Organic Molecules. Photochemistry and Photobiology. 2012; 88(4): 1033-.
41. Zheng Q, Juette MF, Jockusch S, Wasserman MR, Zhou Z, Altman RB*, et al.* Ultra-stable organic fluorophores for single-molecule research. Chem Soc Rev. 2014; 43(4): 1044-56.
42. Jonathan F. Lovell TWBL, Juan Chen,and Gang Zheng. Activatable Photosensitizers for Imaging and Therapy. Chem. Rev. . 2010; 110,5.

Figure legends

Figure 1. Characterizations of CQDs.

(A) TEM images of CQDs, (inset, high resolution TEM images); (B) Size distributions of CQDs; (C) UV-vis absorption spectra of the CQDs; (D) The FL spectrum of the CQDs with excitation wavelengths from 400 nm to 500 nm in 20 nm increments; (E, F) Raman spectra of CQDs and FTIR spectra of CQDs.

Figure 2. XPS spectra of CQDs.

(A) Full scale XPS spectra of the CQDs; (B) High-resolution of C 1s spectrum; (C) high-resolution of N 1s spectrum; (D) High-resolution of O 1s spectrum.

Figure 3. Application of CQDs.

(A) CLSM imaging of HeLa cells labeled with CQDs; (B) In vitro cytotoxicity test of CQDs; (C) Relative viability of HeLa cells incubated with control solution or CQDs (200 $\mu g \cdot mL^{-1}$) and exposed to blue light (460 nm, 30 $mW \cdot cm^{-2}$) for 5 min, 10 min and 15 min. (* $P < 0.05$)

Figure 4. The intracellular ROS generation.

(A) Fluorescence images of HeLa, (a) Bright field transmission image, (b) CQDs fluorescence image collected in the range of 400-450 nm, (c) ROS detection reagent fluorescence image captured in the range of 510-530 nm, and (d) are the merged image; (B) The intracellular ROS production for various concentrations of CQDs with

irradiation for 15 min or without; (C) A simplified energy level diagram shows potential fluorescence and cell death energy transfer pathways. (S0, ground state of the fluorophore molecule; S1, first singlet excited state; Sn (n > 1); T1, first triplet excited state; Ex, excitation by photon absorption; FL, fluorescence).

Supplementary Figure S1

Figure S1. A summary of the micro plasma processing system.

Figures

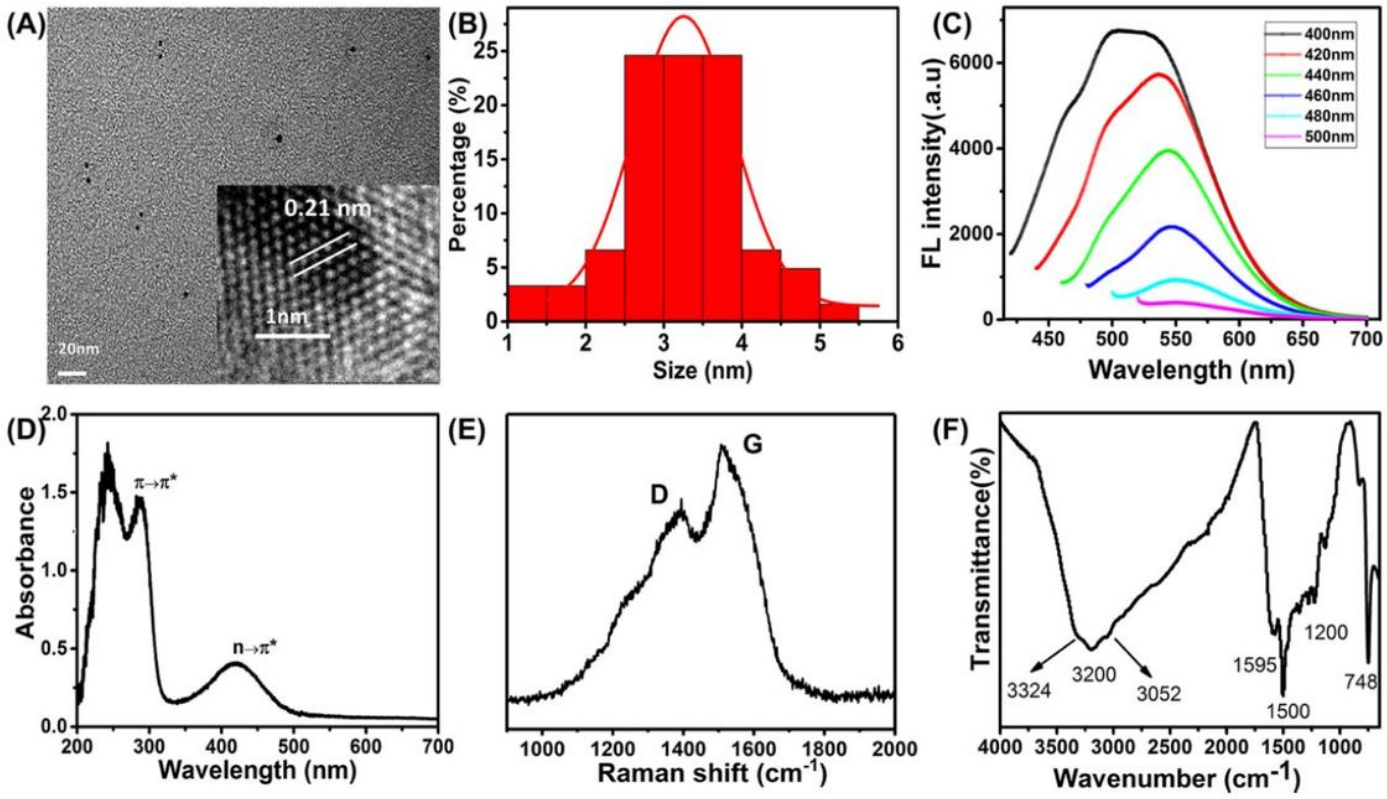

Figure 1

Characterizations of CQDs. (A) TEM images of CQDs, (inset, high resolution TEM images); (B) Size distributions of CQDs; (C) UV-vis absorption spectra of the CQDs; (D) The FL spectrum of the CQDs with excitation wavelengths from 400 nm to 500 nm in 20 nm increments; (E, F) Raman spectra of CQDs and FTIR spectra of CQDs.

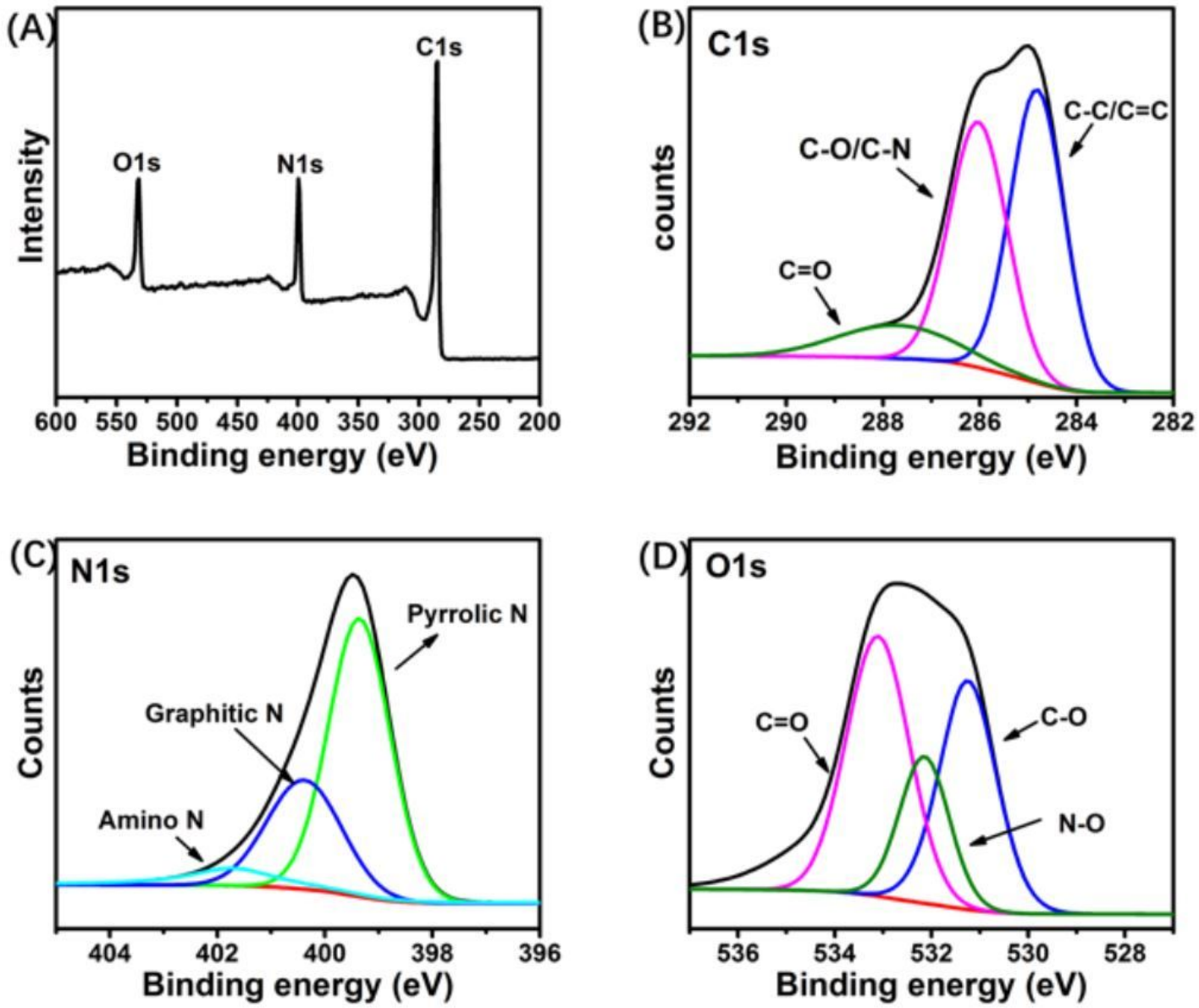

Figure 2

XPS spectra of CQDs. (A) Full scale XPS spectra of the CQDs; (B) High-resolution of C 1s spectrum; (C) high-resolution of N 1s spectrum; (D) High-resolution of O 1s spectrum.

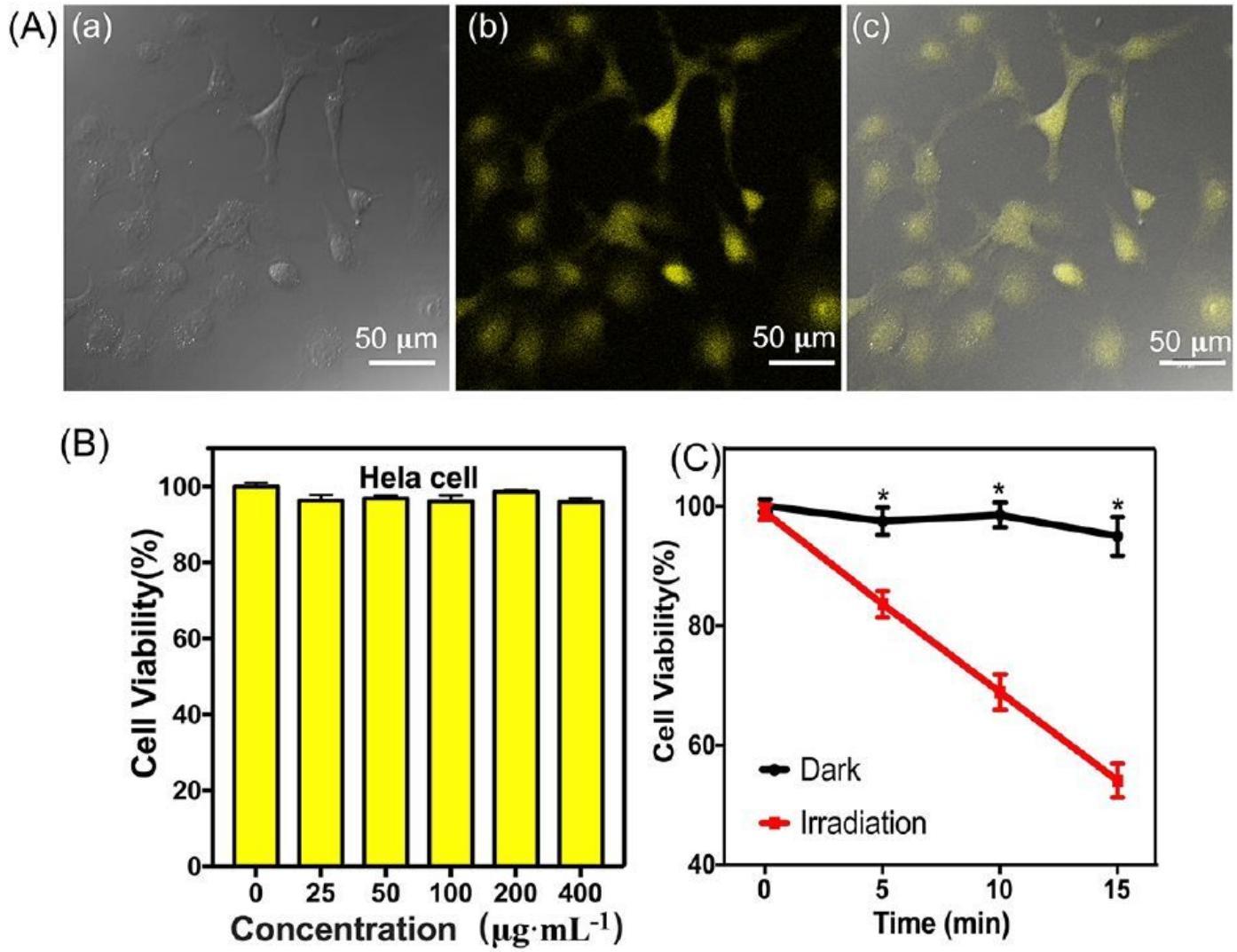

Figure 3

Application of CQDs. (A) CLSM imaging of HeLa cells labeled with CQDs; (B) In vitro cytotoxicity test of CQDs; (C) Relative viability of HeLa cells incubated with control solution or CQDs (200 μg·mL-1) and exposed to blue light (460 nm, 30 mW·cm-2) for 5 min, 10 min and 15 min. (* $P < 0.05$)

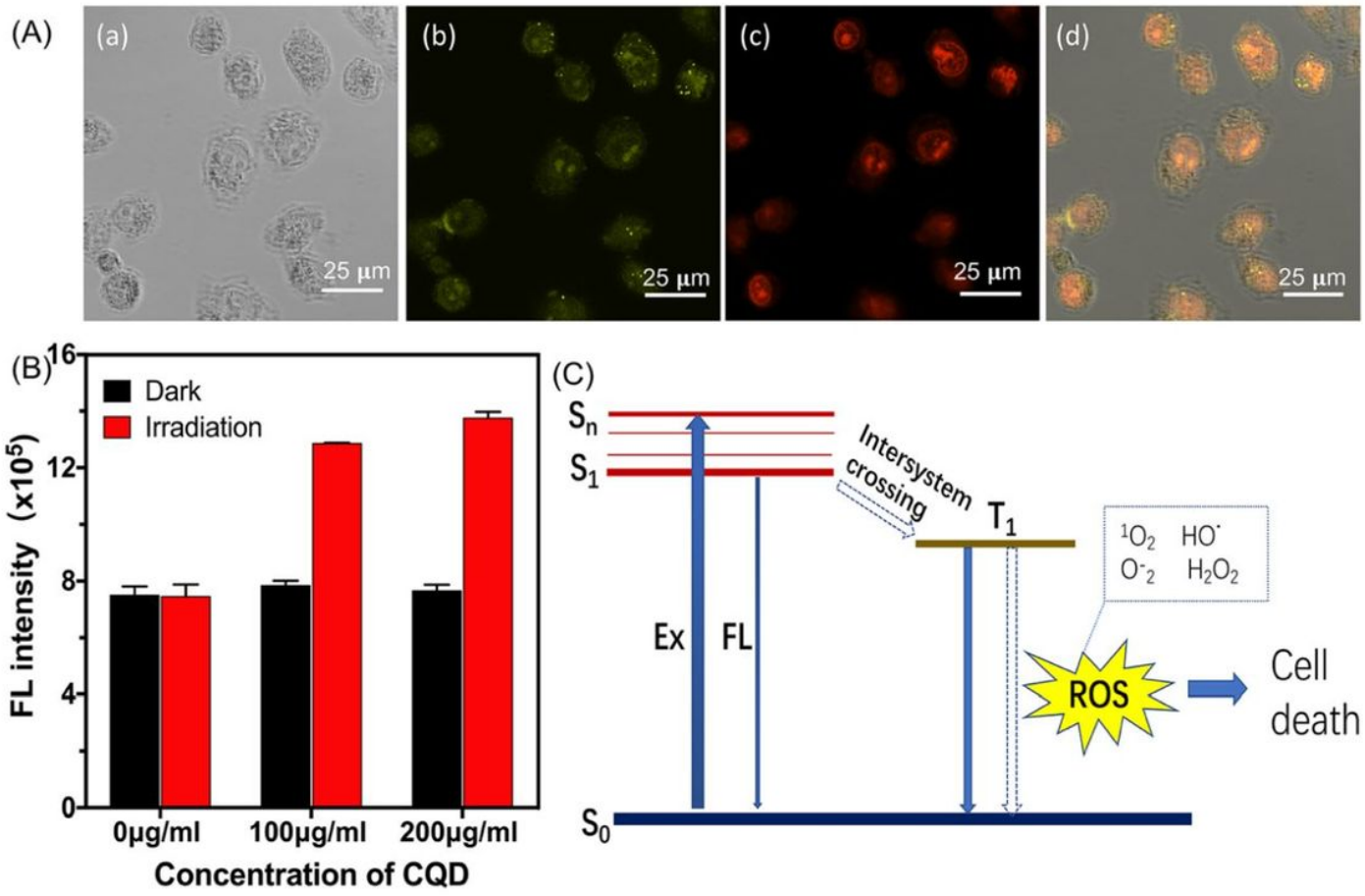

Figure 4

The intracellular ROS generation. (A) Fluorescence images of HeLa, (a) Bright field transmission image, (b) CQDs fluorescence image collected in the range of 400-450 nm, (c) ROS detection reagent fluorescence image captured in the range of 510-530 nm, and (d) are the merged image; (B) The intracellular ROS production for various concentrations of CQDs with irradiation for 15 min or without; (C) A simplified energy level diagram shows potential fluorescence and cell death energy transfer pathways. (S0, ground state of the fluorophore molecule; S1, first singlet excited state; Sn (n > 1); T1, first triplet excited state; Ex, excitation by photon absorption; FL, fluorescence).

Supplementary Files

This is a list of supplementary files associated with this preprint. Click to download.

- FigureS1.pdf